EasyChair Preprint

№ 9166

Characterization of Macroscopic Local Deformation Behavior of Thermo-Mechanically Graded High Strength Aluminum and Steel Alloys

Emad Scharifi, Sebastian Hirte, Steffen Lotz, Michael Mlynek, Ursula Weidig, Agim Ademaj and Kurt Steinhoff

October 26, 2022

Characterization of macroscopic local deformation behavior of thermo-mechanically graded high strength aluminum and steel alloys

Emad Scharifi[1, a *], Sebastian Hirte[1, b], Steffen Lotz[1,2, c], Michael Mlynek[2, d], Ursula Weidig[1, e], Agim Ademaj[2, f] and Kurt Steinhoff[1, g]

[1]University of Kassel, Metal Forming Technology, Kurt-Wolters-Straße 3, 34125 Kassel, Germany

[2]METAKUS Automotive GmbH, Department of Research and Development, Fehrenberger Straße 1a, 34225 Baunatal, Germany

[*a]emad.scharifi@uni-kassel.de, [b]sebastian.hirte@uni-kassel.de, [c]steffen.lotz@uni-kassel.de, [d]michael.mlynek@metakus.com, [e]ursula.weidig@uni-kassel.de, [f]agim.ademaj@metakus.com, [g]steinhof@uni-kassel.de

Keywords: Aluminium, Steel, Functional gradation, Differential cooling, Macroscopic local deformation

Abstract. In this study, the local deformation behavior of the transition zone of thermo-mechanically graded boron steel 22MnB5 and high strength aluminum alloy AA7075 is investigated using an in-situ approach. For this aim, forming tool segments are differentially heated in order to obtain locally tailored microstructures and dissimilar mechanical properties based on the process-induced microstructural phenomena. Material strength distribution is examined by Vickers hardness measurements after thermo-mechanical processing. Tracking of the material- and geometry-dependent local deformation behavior of the resulted transition zone is performed by tensile tests coupled with digital image correlation technique. The experimental results reveal within the transition zone a characteristic reversed S-shape hardness distribution, similar to a sigmoidal curve. The local deformation characterization indicates the occurrence of plastic deformation mainly in the soft zones at the heated forming tools segments, while the harder zones at the cooled tool segments exhibit only an elastic deformation and remain undeformed. By comparing the macroscopic local deformation evolution shortly before failure, absolute strain values up to $\varepsilon_{\text{von Mises}} = 0.62$ and $\varepsilon_{\text{von Mises}} = 0.28$ and a distinct reduction in the area are obtained for 22MnB5 and AA7075, respectively. The occurred plastic strain pattern show the formation of shear bands after a homogenous localization at the necking point.

Introduction

In the field of metal forming technology, the adjustment of graded properties can be accomplished for hardenable steel materials by the combination of locally controlled thermal distribution and forming at elevated temperatures [1]. Therefore, in the framework of hot stamping of boron steel sheets different process variants based on thermo-mechanical approaches are proposed to gain dissimilar mechanical properties as well as microstructure distribution [2,3]. One of the promising techniques is the so-called differential cooling, which can be performed by differentially heated forming tools to provide locally varying cooling rates [2].

By applying this concept to boron steel 22MnB5, the local cooling rates above 30 °C/s at cooled forming tool segments result in a martensitic microstructure with a tensile strength of 1500 MPa,

whereas lower local cooling rates lead to the formation of ductile zones, i.e., ferrite and pearlite with tensile strengths of 614 MPa [2,4]. This shows that the forming tool temperature plays a key role in determining specific microstructural properties for hardenable steel materials after austenitization. Using tool segment temperatures of 25 °C and 400 °C, a significant reduction of 52 % of hardness level from hard to soft is obtained within the transition zone, [5]. Further studies with tensile tests in combination with digital image correlation (DIC) technique gain insight into the plastic deformation behavior of graded components and visualize the failure location for the calibration of finite element (FE) simulations [4,6,7]. To ensure the occurrence of plastic deformation within the gauge length due to the dissimilar hardness distribution, tapered tensile sample geometries with different gauge section widths are used [4]. The experimental results reveal higher total displacement up to failure with increasing the gauge section widths. DIC measurements and FE-simulations show two competing zones for necking initiation at the tensile specimen surface, as a result of the strain hardening. However, a detailed analysis and visualization of local plastic deformation of the graded parts during tensile test is not considered. Therefore, tapered as well as standard tensile test specimen geometries are used in [8] to characterize the local deformation behavior of differentially cooled boron steel 22MnB5 after hot stamping. The DIC measurements reveal for the graded as well as for the martensitic structures higher local logarithmic strain within the necking zone compared to the soft ferritic pearlitic structures. In addition, using a standard tensile test specimen geometry reveals different types of strain localization and failure for the graded structure due to its complex hardening behavior and mixed microstructure leading to multiple necking sites.

Taking the ability of differential cooling to create tailored microstructures in boron steels within one single forming step into the account, this approach is recently proposed also for precipitation hardenable aluminum alloys to obtain dissimilar mechanical properties within one part [9]. Differing cooling rates generated by different tool segment temperatures lead to a characteristic sigmoidal hardness distribution along the longitudinal axes of the formed hat profile. The microstructural investigations based on the electron channeling contrast imaging (ECCI) technique within the transition zone reveal an increase in the precipitate's size with decreasing hardness level. Hence, in the zones of the cooled forming tool segments, a homogenous distribution of fine spherical particles is found, while in the zones of the heated forming tool segments, coarse lath-shaped particles are observed, explaining the obtained hardness distribution. However, despite the reported dissimilar material strength and the variation of microstructural features of the differentially cooled parts their local deformation behavior as well as their tensile deformation performance is not discussed in literature.

For this reason, the above reported open quotations, especially regarding the plastic deformation behavior of the transition zone, inspire the present study to characterize the macroscopic local deformation behavior of thermo-mechanically graded microstructures using DIC technique to highlight the logarithmic local strain fields of the transition zone. For this aim, dfferentially cooled ultra-high-strength boron steel 22MnB5 and high strength aluminum alloy AA7075 are compared to address aspects related to different materials and microstructural mechanisms like diffusionless transformation and precipitation hardening. Hence, relations between process, microstructure and deformation properties will be established with regard to the inhomogeneous microstructure and dissimilar mechanical properties.

Experimental procedure

Materials. The experimental investigations in this study are carried out on boron steel 22MnB5 and high strength aluminum alloy AA7075. The as received condition of 22MnB5 (ArcelorMittal) is Al–Si coated consisting of ferritic and pearlitic structure, an ultimate tensile strength (UTS) of

610 MPa and an elongation after failure of A = 20 %. The as received T6-condition (solution heat treated, quenched, and artificially aged peak strength) of AA7075 (Al–Zn–Mg(–Cu)) shows a hardness of 190 HV and UTS of 580 MPa, respectively. Both materials are sectioned into blanks of 250 mm x 140 mm x 1.5 mm for the hot stamping experiments. A table of the detailed chemical composition of the selected materials is given in [8,9].

Thermo-mechanical forming process and heat treatment. The experimental set-up consists of a roller hearth furnace (type VKR 2800/e , Wärmebehandlungsanlagen für Industrie und Umwelttechnik GmbH (WMU)), a manual transfer to a hydraulic press (type DS 400 Z 160, MAE Maschinen GmbH) equipped with a segmented hat-shaped forming tool and a chamber furnace with radiation heating (type KM70/13, ThermoConcept GmbH) for artificial aging treatment. The forming tool consists of two segments thermally separated by an air gap, in which one segment allows temperatures up to 700 °C whereas the other segment is cooled to a constant temperature of 24 °C by an integrated water-cooling circulation system. The chosen forming speed for all experiments was set to 48 mm^{-1} with a forming force of 1000 kN.

The first group of experiments, Table 1, aims to investigate the local deformation behavior of the transition zone of boron steel 22MnB5. For this purpose, the sectioned 22MnB5 sheets were first austenized at the soaking temperature of T_s = 870 °C and then soaked for t_s = 90 s to obtain a homogenous austenitic structure. The furnace temperature was set to T_F = 930 °C and the sheet temperature was recorded using thermocouples. Subsequently after the austenitization, the heated 22MnB5 sheets were transferred within 6 s to 8 s to the differentially tempered forming tool with T_{FT} = 24 °C and T_{FT} = 500 °C and then formed and held for $t_{Ht,\,FT}$ = 10 s within the closed forming tool.

The second group of experiments focuses on the local deformation behavior of high strength aluminum alloy AA7075 after solution heat treatment, differential cooling and artificial aging, Table 1. For this aim, the sectioned AA7075 sheets were heated to the soaking temperature of T_s = 480 °C to dissolve all alloying elements, formed and cooled within differentially tempered forming tools of T_{FT} = 24 °C and T_{FT} = 350 °C for $t_{Ht,\,FT}$ = 30 s after a manual transfer of 6 s to 8 s. Immediately after forming and cooling the parts were additionally quenched in water to obtain high cooling rates. Finally, the formed parts were artificially aged at T_{AA} = 120 °C for t_{AA} = 20 h to obtain full strength.

Table 1: Selected parameters for different thermo-mechanical processes to obtain tailored microstructure.

Material	Soaking temperature [°C]	Soaking time [s]	Tool temperature heated zone [°C]	Tool temperature cooled zone [°C]	Holding time within closed tools [s]	Aging
22MnB5	870	90	500	24	10	-
AA7075-T6	480	900	350	24	30	120 °C – 20 h

Property characterization and local strain measurement. Vickers hardness measurements (EMCO DuraScan) along the longitudinal axes of the formed parts were carried at a test load of 98.07 N (HV10) for 22MnB5 and 49 N (HV5) for AA7075, respectivly. The measured hardness profiles were then used to highlight the property distribution and to select the position of the extraction of the tensile specimen at the top side of the formed hat profile, Figure 1. Tensile test specimens, matched and aligned to the length of the transition zone were subsequently machined by electric discharge machining with a length 20 mm and width 7 mm [10]. The tensile properties

were then determined with a screw driven uniaxial tensile testing machine (Hegewald & Peschke, max. press capacity: 100 kN) and an extensometer attached on the back side of the tensile specimen. In order to determine the geometrical changes as well as to determine the local strain field of the transition zone, 3D-DIC measurements coupled with tensile tests were carried out. The required surface pattern for DIC was applied using white spray to obtain a homogeneous uniform white background and subsequently black spray to adjust the spot pattern. In case of 22MnB5 the Al-Si coating was removed in advance. For the 3D-strain measurement, two CCD cameras (type Xenoplan 2.8/50-0511, Schneider Kreuznach) with a resolution of 1280 x 1024 pixel at the rate of 10 Hz were focused from different angles on the tensile specimen surface and the measurement zone (transition zone). Finally, data analysis was carried out by ARAMIS software V.6.1 (GOM – Gesellschaft für Optische Messtechnik mbH, Germany).

Results

Effect of differential cooling on property distribution. The effect of differential cooling during hot stamping on ultra-high-strength boron steel 22MnB5 and high strength aluminum alloy AA7075 is presented in Figure 1 (a – b). The hardness distribution along the longitudinal axes of both hat profile reveals a characteristic sigmoidal trend from hard to soft zone, as also reported in the literature [9,11]. In case of 22MnB5, a decrease in hardness level from the hard to soft zone of 480 HV10 to 200 HV10 is measured, revealing the fundamental influence of forming tool temperatures on the material strength, Figure 1 (a). Hence, high cooling rates at cooled tool segments results in a martensitic structure, referring to the high material strength, while lower cooling rates in the heated tool segments causes a soft ferritic pearlitic structure.

Compared to 22MnB5, the same characteristic distribution with a lower hardness level is obtained for AA7075 after differential cooling and artificial aging, Figure 1 (b). It reveals a clear transition and decrease of material hardness from 185 HV at the cooled tool segment to 100 HV at the heated tool segment. Thus, the creation of tailored microstructure distribution with a corresponding significant change in material strength within one part is also possible for precipitation hardenable aluminum alloys by means of locally differing contact cooling rates after solutionizing. Finally, a measured transition zone length of 20 mm is found for both 22MnB5 and AA7075.

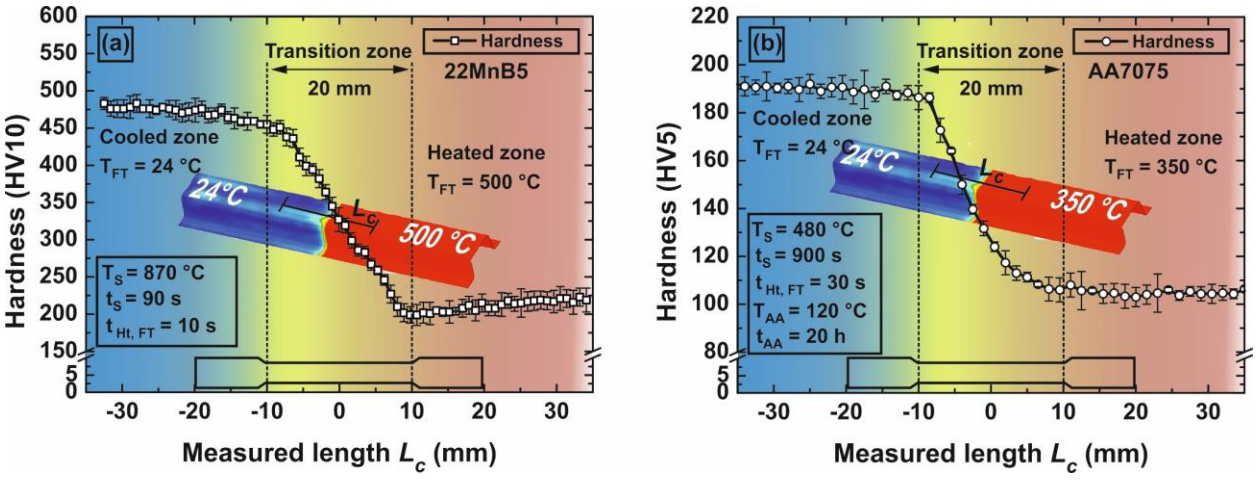

Figure 1: Hardness profile after differential cooling for (a) 22MnB5 and (b) AA7075.

Effect of differential cooling on tensile deformation performance. In addition to the hardness profile, tensile tests demonstrate the plastic deformation behavior of the transition zone of 22MnB5 and AA7075, Figure 2 (a – b). For 22MnB5, after attaining the YS of 460 MPa, the

tensile stress increases to an UTS of 685 MPa on average due to the high strain hardening of 22MnB5, Figure 2 (a), whereas the elongation after failure, as indicator for ductility properties, reaches a maximum value of 7.4 %.

The tensile deformation performance of AA7075 after differential cooling and artificial aging shows Figure 2 (b). The obtained YS of 375 MPa and UTS of 491 MPa are lower than the values of the as received T6-condition whilst the elongation after failure amounts to a maximum value of 6.5 %.

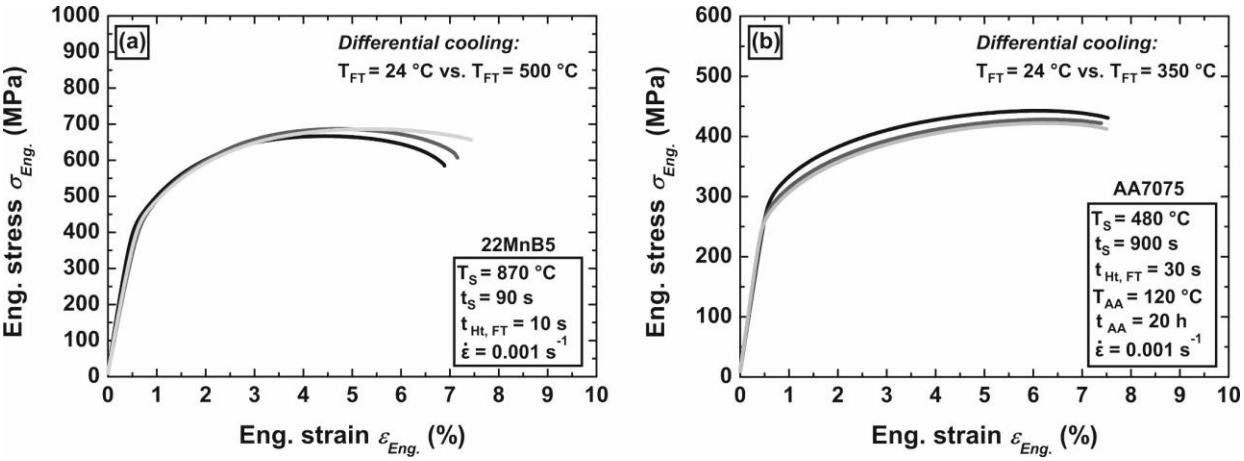

Figure 2: Tensile deformation of the transition zone of (a) 22MnB5 and (b) AA7075.

Characterization of macroscopic local deformation behavior. The macroscopic local deformation evolution and the related logarithmic von Mises strain map during tensile tests of the transition zone of 22MnB5 and AA7075 after differential cooling is depicted in Figure 3 (a – d). For both, plastic deformation appears mainly within the soft region, respectively heated forming tool segment zone. Figure 3 (a) shows the logarithmic von Mises strain evolution for 22MnB5 within the transition zone during tensile deformation. At the beginning of plastic deformation and at the first stage of Eng. strain of $\varepsilon_{Eng.}$ = 2.0 %, a slight difference in logarithmic von Mises strain in the cooled and heated zones along the measured length L_c can be seen. Accordingly, plastic deformation occurs mainly in the softer zones at the heated tool segments, while the harder zones at the cooled tool segments exhibit only an elastic deformation. With increasing the Eng. strain, plastic deformation occurs mainly in the heated tool zone, with this characteristic prevailing up to the necking point as well as to fracture. After the neck at $\varepsilon_{Eng.}$ = 4.0 %, high localized logarithmic strain up to failure of $\varepsilon_{von\ Mises}$ = 0.62 and a significant reduction in area is obtained for 22MnB5. The progression of the local logarithmic von Mises strain map in Figure 3 (b) reveals and confirms the obtained local deformation evolution in Figure 3 (a). It further can be deduced that the occurrence of plastic deformation is limited to the softer zones at the heated tool segments, which develop a strong strain localization leading to failure of the tensile specimen in the highly formed region with increasing plastic strain. Hence, within the transition zone of 22MnB5 the occurrence of plastic deformation during tensile tests underlies a well-defined delimitation. However, in contrast to the investigation in [8] multiple necking phenomena and a change of deformation locations after necking is not observed for the same used tensile specimen geometry.

Figure 3 (c) shows the progression of the local strain until failure within the transition zone of AA7075 during tensile test. It reveals a similar logarithmic von Mises strain distribution compared to 22MnB5, Figure 3 (a). From the initial stage of Eng. strain of $\varepsilon_{Eng.}$ = 2.0 % and up to the necking point as well as to failure, local plastic strain is measured predominantly in the softer zone at the

heated tool segment. After the neck at an Eng. strain of $\varepsilon_{Eng.}$ = 5.5 %, a maximum localized logarithmic strain of $\varepsilon_{von\ Mises}$ = 0.28 is obtained within the area of failure. It is worth to note that in case of AA7075, failure occurs subsequently and shortly after attaining the necking point and the load-supporting zone decreases rapidly, as shown in the local logarithmic von Mises strain map in Figure 3 (d). However, plastic deformation also occurs in the zone at the cooled tool segment, which is comparatively lower to the measured logarithmic strain at the heated zone. This behavior shows also Figure 3 (d), presenting the local logarithmic von Mises strain map. Nevertheless, this plastic deformation takes place only to a limited extent at areas of the cooled tool segment close to the heated tool segment, whilst the majority of this zone with higher hardness values remains undeformed up to failure.

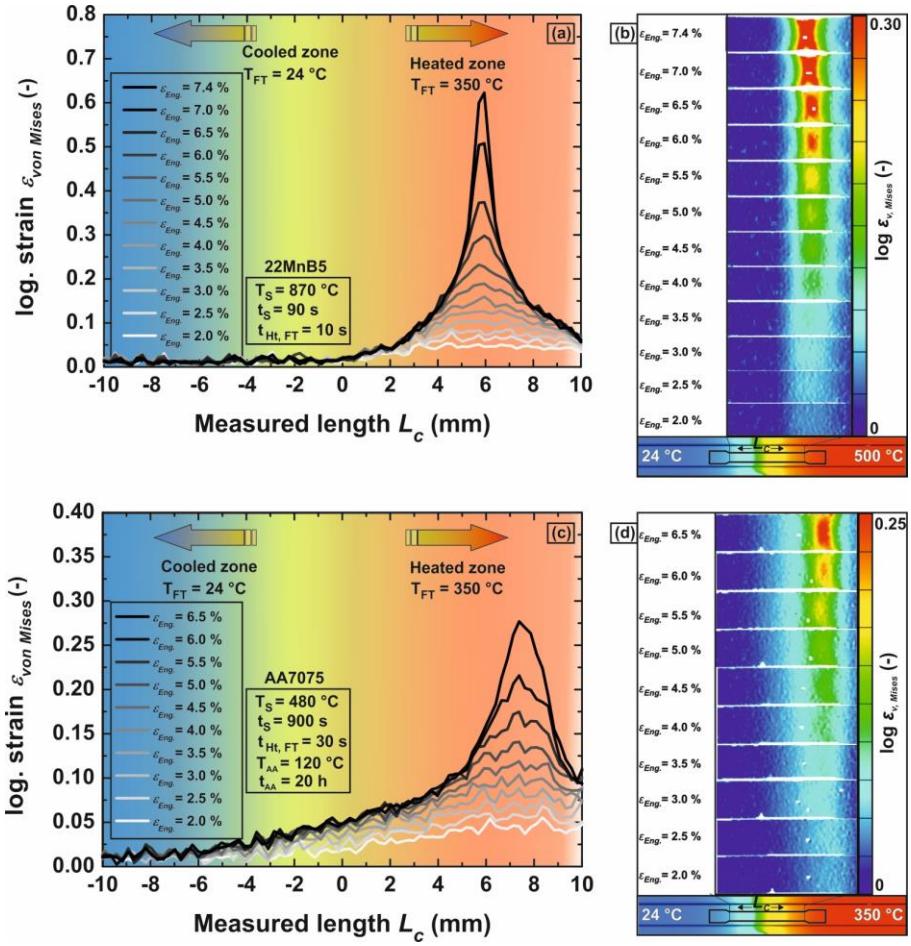

Figure 3: Local deformation behavior and the corresponding deformation profile maps along the tensile direction within the transition zone of (a – b) 22MnB5 and (c – d) AA7075 during tensile test.

The progression of the local strain at different specific locations on the tensile specimen of 22MnB5 and AA7075 and the corresponding logarithmic von Mises strain map until failure shows Figure 4 (a – b). The first position (position 1) is located in the center of the specimen, where the highest logarithmic von Mises strain value occurs. The second position (position 2) is situated at the same height but left of position 1. The third position (position 3) is chosen at 1.2 mm above position 2. The tracking of the evolution of the local strain at 3 different positions of the transition zone intends to identify the type of failure and the nucleation of shear bands during the tensile test immediately before the occurrence of failure. The resulted logarithmic von Mises local strain of the different positions reveal for both, 22MnB5 and AA7075 that the highest strain appear in the

center of the tensile specimen and exactly at the point where necking was initiated. In the course of the plastic deformation and after the neck initiation of 22MnB5, two crossed shear bands occur, which results in a higher logarithmic von Mises local strain for position 3 compared to position 2, Figure 4 (a). This behavior is also observed for AA7075, Figure 4 (b), although the resulting local strain is not as pronounced as for 22MnB5.

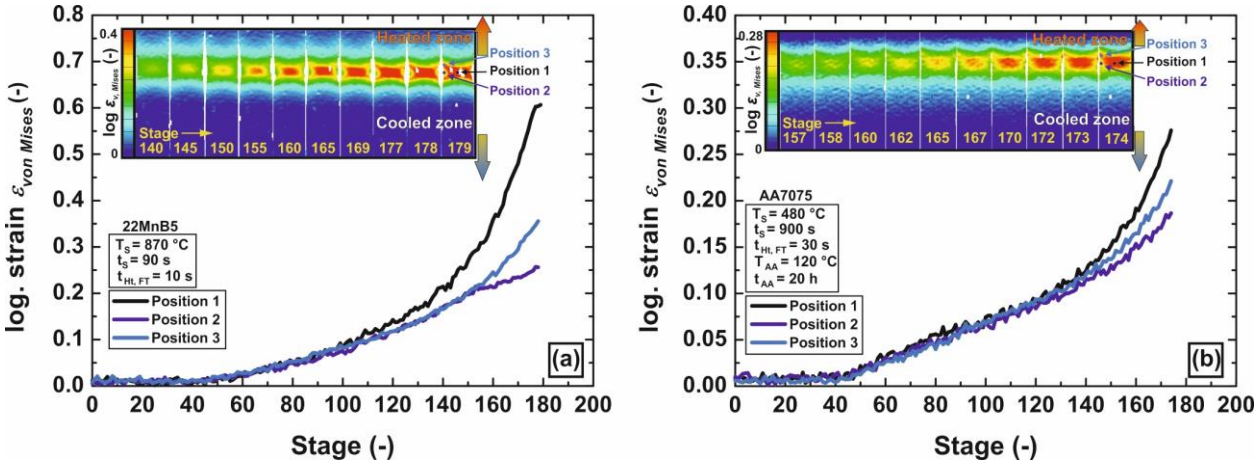

Figure 4: Progression of the local strain and the corresponding logarithmic von Mises strain map for (a) 22MnB5 and (b) AA7075.

Discussion and Conclusion

The present study investigates the local deformation behavior of the transition zone of thermo-mechanically graded boron steel 22MnB5 and high strength aluminum alloy AA7075 after differential cooling. After this thermo-mechanically gradation of 22MnB5 and AA7075 the obtained hardness distribution reveals the characteristic reversed S-shape. For 22MnB5, this property distribution is a result of the change in transformation mechanisms, i.e. from diffusionless lattice shearing to diffusion-controlled transformation, leading to a hard martensitic structure and a soft ferritic-pearlitic phase after differential cooling using segmented forming tools after uniform austenitization. Hence, from the hardness profile in Figure 1 (a – b), a gradual change of present phases from hard martensite to soft ferrite–pearlite is derived. In case of high strength aluminum alloy AA7075, similar to 22MnB5, high cooling rates results in high material strength and low cooling rates to significantly lower material strength. This behavior is linked to a specific change in the microstructure, which is created by thermo-mechanically induced precipitation of particles or suppression of it during the differential cooling. At the low tool segment temperature of T_{FT} = 24 °C, the nucleation and growth of precipitates is suppressed leading to a high level of supersaturation in the solid solution. Hence, after artificial aging, the formation and growth of semi-coherent strengthening η´-phases explain the obtained high hardness level in the cooled zones. In contrast, forming at a higher forming tool segment temperature of T_{FT} = 350 °C together with an isothermal holding of 30 s leads to precipitation already during forming enabled by the sufficient thermal energy at 350 °C and results in a decreased level of supersaturation. During the following artificial aging the formation and growth of lath-shaped metastable η-phases is promoted. The resulted coarse particles hardly contribute to the yield strength increase and their interaction with moving dislocation is identified by the bypass mechanisms. Within the transition zone the gradual change of the supersaturation in the solid solution state possibly leads to mixed-precipitate structures and a gradual amount of growing fine precipitates. This may be the reason for the continuous decrease of hardness values from hard to soft.

The progression of the local strain and the related logarithmic von Mises strain map during tensile deformation show the occurrence of plastic deformation mainly in the zones at the heated forming tool segments, i.e. soft zones, while the hard zones at the cooled forming tool segments remain almost undeformed. The explanation for this behavior can be found in the specific microstructure of the soft zones, exhibiting lower yield strength compared to the harder zone, which enables and eases the initiation and accumulation of plastic deformation and movement of dislocations due to the high local stress concentration. These phenomena lead to higher formability of the soft zone and concomitantly to high strain hardening. On top of that, due to the local deformation concentration in limited regions, the plastic instability after the necking point and the occurrence of crossed shear bands leads to a further increase of the amount of local plastic deformation. Therefore, local plastic strain as shown in Figure 3 (a) for 22MnB5 accumulates as a result of plastic flow under plane stress domination and lead to significant high local logarithmic von Mises strain values at the necking zone short before failure. Due to the tailored mechanical properties by different microstructural features, the generation and propagation of necking as well as the failure can be controlled and limited to defined zones. Consequently, the mechanical performance of the mixed microstructure within the transition zone is governed by the macroscopic stress and strain partitioning as can be clearly seen by DIC analysis.

References

[1] K. Steinhoff, New process strategies and resulting product structures by locally induced thermo-mechanical interaction, in: M. Liewald, K. Siegert (Eds.), Neuere Entwicklungen Der Massivumformung., MAT INFO Werkstoff-Informationsgesellschaft mbH, Frankfurt, America, 2005: pp. 277–298.

[2] A. Ademaj, A. Donis, S. Prokoph, U. Weidig, K. Steinhoff, Hot stamping strategies for manufacturing of thermo-mechanically graded parts, in: Proc. 4th Int. Conf. Thermomechanical Process. Sheff., 2012.

[3] M. Merklein, M. Wieland, M. Lechner, S. Bruschi, A. Ghiotti, Hot stamping of boron steel sheets with tailored properties: A review, J. Mater. Process. Technol. 228 (2016) 11–24. https://doi.org/10.1016/j.jmatprotec.2015.09.023.

[4] T.K. Eller, L. Greve, M.T. Andres, M. Medricky, A. Hatscher, V.T. Meinders, A.H. Van Den Boogaard, Plasticity and fracture modeling of quench-hardenable boron steel with tailored properties, J. Mater. Process. Technol. 214 (2014) 1211–1227. https://doi.org/10.1016/j.jmatprotec.2013.12.015.

[5] R. George, A. Bardelcik, M.J. Worswick, Hot forming of boron steels using heated and cooled tooling for tailored properties, J. Mater. Process. Technol. 212 (2012) 2386–2399. https://doi.org/10.1016/j.jmatprotec.2012.06.028.

[6] J. Min, J. Lin, Y. Min, Effect of thermo-mechanical process on the microstructure and secondary-deformation behavior of 22MnB5 steels, J. Mater. Process. Technol. 213 (2013) 818–825. https://doi.org/10.1016/j.jmatprotec.2012.12.012.

[7] P. Srithananan, P. Kaewtatip, V. Uthaisangsuk, Micromechanics-based modeling of stress-strain and fracture behavior of heat-treated boron steels for hot stamping process, Mater. Sci. Eng. A. 667 (2016) 61–76. https://doi.org/10.1016/j.msea.2016.04.065.

[8] E. Scharifi, T. Schade, A. Ademaj, S.V. Sajadifar, U. Weidig, T. Niendorf, K. Steinhoff, Characterization of Mechanical Properties, Macroscopic Deformation Behavior, and Microstructure of Functionally Graded 22MnB5 Steel, Steel Res. Int. 92 (2021). https://doi.org/10.1002/srin.202000633.

[9] E. Scharifi, M. Roscher, S. Lotz, U. Weidig, E. Jägle, K. Steinhoff, Functional Gradation in Precipitation Hardenable AA7075 Alloy by Differential Cooling Strategies, Key Eng. Mater. 883 (2021) 159–166. https://doi.org/10.4028/www.scientific.net/kem.883.159.

[10] E. Scharifi, S.V. Sajadifar, G. Moeini, U. Weidig, S. Böhm, T. Niendorf, K. Steinhoff, Dynamic Tensile Deformation of High Strength Aluminum Alloys Processed Following Novel Thermomechanical Treatment Strategies, Adv. Eng. Mater. 22 (2020) 2000193. https://doi.org/10.1002/adem.202000193.

[11] A. Ademaj, A. Donis, U. Weidig, K. Steinhoff, Hot Stamping of Multi-Material Composites, 4th Int. Conf. Hot Sheet Met. Form. High-Performance Steel. (2013) 401–408.